

1 Controls of groundwater floodwave propagation in a gravelly floodplain

2

3

4

5 Claude-André Cloutier

6 Département de biologie, chimie et géographie, Centre for Northern Studies (CEN)

7 Université du Québec à Rimouski

8 Rimouski, QC, Canada, G5L 3A1

9 Phone : 418-723-1968 # 1733

10 Claude-andre\_Cloutier@uqar.ca

11

12 Thomas Buffin-Bélanger

13 Département de biologie, chimie et géographie, Centre for Northern Studies (CEN)

14 Université du Québec à Rimouski

15 Rimouski, QC, Canada, G5L 3A1

16 Phone : 418-723-1968 # 1577

17 Thomas\_Buffin-Belanger@uqar.ca

18

19 Marie Larocque

20 Département des sciences de la Terre et de l'atmosphère

21 Université du Québec à Montréal

22 C.P. 8888 succursale Centre-ville, Montréal, QC, Canada

23 H3C 3P8

24 Phone: 514-987-3000 # 1515

25 larocque.marie@uqam.ca

26

27

28

29

30 Key Points:

- 31 • A groundwater floodwave can propagate through an alluvial aquifer
- 32 • Streamfloods affect groundwater flow orientation
- 33 • Streamfloods leading to groundwater exfiltration

34

35 Index Terms: Groundwater; Floodplain dynamics; Groundwater – surface water  
36 interaction; Floods

37 Key words: river–groundwater interactions; flood events; groundwater flooding;  
38 groundwater floodwave; flow reversals; floodplain; Matane River (eastern Canada)

39

40 ABSTRACT

41 Interactions between surface water and groundwater can occur over a wide range of  
42 spatial and temporal scales within a high hydraulic conductivity gravelly floodplain. In  
43 this research, dynamics of river-groundwater interactions in the floodplain of the Matane  
44 River (eastern Canada) are described on a flood event basis. Eleven piezometers  
45 equipped with pressure sensors were installed to monitor river stage and groundwater  
46 levels at a 15-minutes interval during the summer and fall of 2011. Results suggest that  
47 the alluvial aquifer of the Matane Valley is hydraulically connected and primarily  
48 controlled by river stage fluctuations, flood duration and magnitude. The largest flood  
49 event recorded affected local groundwater flow orientation by generating an inversion of  
50 the hydraulic gradient for sixteen hours. Piezometric data show the propagation of a well-  
51 defined groundwater floodwave for every flood recorded as well as for discharges below  
52 bankfull ( $< 0.5 Q_{bf}$ ). A wave propagated through the entire floodplain (250 m) for each  
53 measured flood while its amplitude and velocity were highly dependent on hydroclimatic  
54 conditions. The groundwater floodwave, which is interpreted as a dynamic wave,  
55 propagated through the floodplain at 2-3 orders of magnitude faster than groundwater  
56 flux velocities. It was found that groundwater exfiltration can occur in areas distant from  
57 the channel even at stream discharges that are well below bankfull. This study supports  
58 the idea that a river flood has a much larger effect in time and space than what is  
59 occurring within the channel.

60

61

62 1. INTRODUCTION

63 A gravel-dominated floodplain and its fluvial system are hydrologically connected  
64 entities linked by interactions beyond recharge and discharge processes. Woessner (2000)  
65 emphasized the need to conceptualize and characterize surface-water-groundwater  
66 exchanges both at the channel and at the floodplain scale to fully understand the complex  
67 interactions between the two reservoirs. The stream-groundwater mixing zone is referred  
68 to as the hyporheic zone. It is generally understood that surface water-groundwater  
69 mixing exchanges at channel and floodplain scales are driven by hydrostatic and  
70 hydrodynamic processes, the importance of which varies according to channel forms and  
71 streambed gradients (Harvey and Bencala, 1993; Stonedahl et al., 2010; Wondzell and  
72 Gooseff, 2013). The boundaries of the hyporheic zone can be defined by the proportion  
73 of surface water infiltrated within the saturated zone (Triska et al., 1989) or by the  
74 residence time of the infiltrated surface water (Cardenas, 2008; Gooseff, 2010). However,  
75 pressure exchanges between surface water and groundwater can occur beyond the  
76 hyporheic zone, with no flow mixing (Wondzell and Gooseff, 2013). River stage  
77 fluctuations can lead to the generation of groundwater flooding via pressure exchanges.  
78 Groundwater flooding, i.e., groundwater exfiltration at the land surface, is controlled by  
79 several factors in floodplain environments: floodplain morphology, pre-flooding depth of  
80 the unsaturated zone, hydraulic properties of floodplain sediments, and degree of  
81 connectivity between the stream and its alluvial aquifer (Mardhel et al., 2007). Two  
82 scenarios can lead to the rise of groundwater levels resulting in flooding: 1) the complete  
83 saturation of subsurface permeable strata due to a prolonged rainfall and 2) groundwater  
84 level rises due to river stage fluctuations. Concerning the second scenario, Burt et al.

85 (2002) and Jung et al. (2004) noted that once the River Severn (UK) exceeded the  
86 elevation of the floodplain groundwater in summer conditions, the development of a  
87 groundwater ridge was responsible for switching off hillslope inputs at stream discharges  
88 below bankfull. Mertes (1997) also illustrated that inundation of a dry or saturated  
89 floodplain may occur as the river stage rises, even before the channel overtops its banks.  
90 In-channel and overbank floods perform geomorphic work that modifies groundwater-  
91 surface water interactions (Harvey et al., 2012). In contrast, groundwater floodwaves  
92 propagation performs no geomorphic work, but nevertheless can influence riparian  
93 ecology or flooding of humanbuilt systems on floodplains (Kreibich and Thieken, 2008).

94

95 Field studies at the river-reach scale have been carried out to document the hydrological  
96 interactions between river stage and groundwater fluctuations beyond the hyporheic zone  
97 in floodplain environments (e.g., Burt et al., 2002; Jung et al., 2004; Lewandowski et al.,  
98 2009; Vidon, 2012). It has been reported that river stage fluctuations were responsible for  
99 delayed water level fluctuations at distances greater than 300 m from the channel (e.g.,  
100 Verkerdy and Meijerink, 1998; Lewandowski et al., 2009). The process of pressure wave  
101 propagation through the floodplains (Sophocleous, 1991; Verkerdy and Meijerink, 1998;  
102 Jung et al., 2004; Lewandowski et al., 2009; Vidon, 2012) and the direction of exchanges  
103 between groundwater and surface water at the river bed (Barlow and Coupe, 2009) have  
104 has also been documented. However, only a few field studies describe the interactions  
105 between surface water and groundwater on a flood event basis (e.g., Burt et al., 2002;  
106 Jung et al., 2004; Barlow and Coupe, 2009; Vidon, 2012). Moreover, field  
107 instrumentation usually covers only a limited portion of the floodplain with transects of

108 piezometers (Burt et al., 2002; Jung et al., 2004; Lewandowski et al., 2009). The lack of  
109 empirical data on the propagation of groundwater flooding in two dimensions during  
110 several flood events limits our understanding of complex river-groundwater interactions.  
111 Using higher spatial and temporal resolutions is necessary to describe how flow  
112 orientations within alluvial floodplains are affected by flood events. Furthermore, the  
113 processes that generate groundwater exfiltration and the effects of floodplain morphology  
114 on river-groundwater interactions in alluvial floodplains need to be better understood to  
115 facilitate land use management in floodplains.

116

117 The aim of this paper is to document surface water-groundwater interactions in an  
118 alluvial floodplain at high spatial and temporal resolutions at the flood event scale. The  
119 study was carried out on the Matane River floodplain (province of Quebec, Canada). The  
120 Matane Valley is known to experience floods of different types every few years:  
121 overbank flow during snow melt, during rainstorms, or by ice jams. The valley is also  
122 known to experience flooding in areas that are distant from the channel when there is no  
123 overbank flow. An experimental site was instrumented and water levels were monitored  
124 for 174 days in the summer and fall of 2011. Time series analysis was used to interpret  
125 results and provide a detailed picture of the interactions between river and groundwater  
126 levels.

## 127 2. MATERIALS AND METHODS

### 128 *2.1 Study site*

129 The Matane River flows from the Chic-Choc mountain range to the south shore of the  
130 St. Lawrence estuary, draining a 1678 km<sup>2</sup> basin (Figure 1). The flow regime of the  
131 Matane River is nivo-pluvial, with the highest stream discharges occurring in early May.  
132 The mean annual stream discharge is 39 m<sup>3</sup>s<sup>-1</sup> (1929–2009), and the bankfull discharge is  
133 estimated at 350 m<sup>3</sup>s<sup>-1</sup>. Discharge values are available from the Matane gauging station  
134 (CEHQ, 2013; station 021601). The irregular meandering planform flows into a wide  
135 semi-alluvial valley cut into recent fluvial deposits (Lebuis, 1973). The entire floodplain  
136 of the gravel-bed Matane River is constructed by different types of meander growths that  
137 shift over time. The mean channel width and the mean valley width are 55 m and 475 m,  
138 respectively.

139

140 The study site, located 28 km upstream from the estuary (48° 40' 5.678" N, 67° 21'  
141 12.34" W), is characterized by an elongated depression that corresponds to an abandoned  
142 oxbow and a few overflow channels (Figure 1). The site was chosen for its history of  
143 flooding at river stages below bankfull. The floodplain is very low, i.e., at bankfull  
144 discharge, the deepest parts of the depression are lower than the river water level. During  
145 the study period, the mean groundwater level at the study site is 58.8 m above mean sea  
146 level, whereas the surface elevation of the floodplain is 60.4 m above sea level, i.e., the  
147 unsaturated zone is on average 1.4 m. The sediments overlying the bedrock and forming  
148 the alluvial aquifer consist of coarse sands and gravels overtopped by a overbank sand  
149 deposit layers of variable thickness from 0.30 m at highest topographic forms to 0.75 m  
150 within abandoned channels. The unconfined alluvial aquifer thickness is 25 m  
151 according to a bedrock borehole next to the study site.

152 *2.2 Sampling strategy*

153 To investigate hydraulic heads in the floodplain, the local groundwater flows, and the  
154 stream discharge at which exfiltration occurs, an array of 11 piezometers was installed  
155 (Figure 1). Arrays of piezometers have been used with success in previous studies to  
156 document the surface water-groundwater interactions (e.g., Haycock and Burt, 1993; Burt  
157 et al., 2002; Lewandowski et al., 2009; Vidon, 2012). Piezometers are made from 3.8 cm  
158 ID PVC pipes sealed at the base and equipped with a 30 cm screens at the bottom end. At  
159 every location, piezometers reached 3 m below the surface so that the bottom end would  
160 always be at or below the altitude of the river bed. However, because of the surface  
161 microtopography, the piezometers bottom reached various depths within the alluvial  
162 aquifer. Piezometer names correspond to the shortest perpendicular distance between the  
163 piezometer and the river bank. Slug tests were conducted at each piezometer, and rising-  
164 head values were interpreted with the Hvorslev method (Hvorslev, 1951). Results from  
165 the slug tests at each piezometer indicate that hydraulic conductivities are relatively  
166 homogeneous (from  $8.48 \times 10^{-4}$  to  $2.1 \times 10^{-5}$  m s<sup>-1</sup>; Table 1) and representative of coarse  
167 sand to gravel deposits (Freeze and Cherry, 1979).

168

169 Data were collected from 21 June to 12 December 2011. This period correspond roughly  
170 to the end of the long spring flood to the beginning of winter low flow period where flow  
171 stage is influenced by the formation of an ice cover. From 21 June to 7 September 2011,  
172 eight piezometers were equipped with pressure transducers (Hobo U20-001) for  
173 automatic water level measurements at 15 min intervals. Three more pressure transducers  
174 were added at piezometers D139, D21, and D196 starting on 7 September. Two river

175 stage gauges were installed on the riverbed, downstream and upstream of the study site  
176 (RSGdn and RSGup; Hobo U20-001) to monitor water levels in the Matane River every  
177 15 minutes over the complete study period. Piezometer locations were measured using a  
178 Magellan ProMark III differential GPS. A LIDAR survey with a 24 cm resolution  
179 (3.3 cm accuracy) was used to obtain a high resolution map of topography. Precipitation  
180 was measured with a tipping bucket pluviometer located on site (Hobo RG3-M).

181

### 182 *2.3 Data analysis*

183 During the data collection period, water levels and river stages were never lower than the  
184 piezometer and RSGup data loggers. However, river stages at RSGdn occasionally  
185 dropped below the data logger, so time series at this location are discontinuous. The  
186 RSGdn time series was only used to analyze the 5–12 September event.

187

188 During flood events, the timing of maximum water level elevation differed between the  
189 piezometers and the river gauge. To determine the time lags between time series of river  
190 stages and piezometer water levels, cross-correlation analyses were performed. Cross-  
191 correlation analyses between time series of piezometric levels, river levels, and  
192 precipitation were also used to provide information on the strength of the relationships  
193 between input and output processes and also on the time lag between the processes.  
194 Analyses were performed with the PAST software (Hammer et al., 2001) on the times  
195 series from piezometer water levels and from the RSGup for each event. Due to the  
196 distance of only 400 m between river gauges, there was no significant lag between  
197 RSGup and RSGdn data that would cause lower lag between the surface-groundwater

198 using a rebuilt RSGdn time series from RSGup data. The time lag corresponds to the  
199 delay at which the maximum correlation coefficient occurred between two time series.

200

### 201 3. RESULTS

#### 202 *3.1. Cross-correlation analysis of water level fluctuations*

203 Time series of water levels and river stages indicate a strong synchronicity of the  
204 groundwater and river systems. Figure 2 shows the time series of water levels for all  
205 piezometers and for the river stage gauge upstream (RSGup) at a 15 min interval for the  
206 period of 21 June to 12 December 2011. During this period, seven floods below bankfull  
207 discharge occurred. The largest flood took place from 5–12 September, with a maximum  
208 stream discharge of  $213 \text{ m}^3 \text{ s}^{-1}$  on September 6 at 2:00pm (all times are reported in local  
209 time, EDT) (60% of  $Q_{\text{bankfull}}$ ). The six other floods ranged from 29 to  $72 \text{ m}^3 \text{ s}^{-1}$ . The 5–12  
210 September flood event induced water level fluctuations of 1.14 and 0.68 m at piezometers  
211 D21 and D257, respectively. Figure 2 shows river levels are always higher than hydraulic  
212 heads. This is explicated by the river stage gauge that is located 400 m upstream from the  
213 study site (RSGup). The highest water levels were usually observed at piezometers  
214 distant from the river (D223–D257) and the lowest were close to the river (D21–D25), so  
215 the Matane river is generally a gaining stream.

216

217 Figure 3 presents cross-correlation functions between river levels as input processes and  
218 groundwater levels as output processes as well as cross-correlation functions between  
219 precipitation and groundwater levels for the 2–16 July event. The results reflect the  
220 strong relationship ( $r > 0.9$  at maximum correlation) between the river stage fluctuations

221 and the groundwater level fluctuations at every piezometer. With values ranging from  
222 0.89 to 0.98, and 8 correlations out of 11 being higher than 0.95, the cross-correlation  
223 results suggest that groundwater levels are strongly correlated with river stage  
224 fluctuations. The precipitation–groundwater level correlations (0.2 - 0.3) are significantly  
225 lower than the river–groundwater level correlations. This gives strong evidence that the  
226 input signal from precipitation is significantly reduced by the large storage capacity of  
227 the unsaturated zone.

228

229 Time lags between inputs and outputs derived from the cross-correlation analysis reveal  
230 the spatiotemporal response of the groundwater level to the rising stream discharge or to  
231 the precipitation. For the 2–16 July event, time lags between precipitation and  
232 groundwater levels (at maximum correlation) varied from 22 to 44 hours while time lags  
233 between river stage and groundwater levels varied from 1 to 22 hours. In both cases, the  
234 shorter time lags are associated with piezometers located closer to the river. The longer  
235 precipitation-groundwater level time lags reveal a significant storage capacity of the  
236 unsaturated zone during precipitation, and the shorter river-groundwater level time lags  
237 are interpreted as an indication that groundwater fluctuations are associated with river  
238 level fluctuations.

239

240 Figure 4 shows the relationship between the time lags from the river level-groundwater  
241 level cross-correlation analysis and the piezometer distance from the river for three flood  
242 events. A strong linear relationship emerges between the two variables as shown by the

243 strong  $R^2$  for the regression model for the three flood events (all  $R^2$  values are higher than  
244 0.91). The scatter for each event may be due to the fact that the piezometers are not  
245 perfectly aligned (see Figure 1c). The figure also shows that at 250 m the highest  
246 groundwater level is reached 25 h later than the highest river stage for the September  
247 flood event, but 40 h later for the November flood event. This reveals contrasting  
248 propagation velocities for the groundwater crest moving throughout the floodplain. An  
249 average propagation velocity can be estimated from the slope coefficient of the regression  
250 lines. For the selected flood events, the propagation velocities range between  $6.7 \text{ m h}^{-1}$   
251 and  $11.5 \text{ m h}^{-1}$ . It can be noted that the two largest floods present a similarly high  
252 propagation velocity while the lowest flood is linked with the smallest propagation  
253 velocity.

254

255 The relative homogeneity of hydraulic conductivities over the floodplain shows that the  
256 spatial distribution of lag values over the study site cannot be caused by floodplain  
257 morphology. Comparison of hydraulic conductivity values to the floodplain elevation  
258 (Table 1) also shows that spatial distribution of hydraulic conductivities is not explained  
259 by the floodplain morphology. Moreover, if direct groundwater recharge or hillslope  
260 runoff processes were responsible for groundwater level fluctuations, a large variability  
261 of lag values among piezometers would not be obtained for every flood event. Relations  
262 between time lags and peak stream discharge values and between time lags and rising  
263 limb times were investigated and no significant relationships emerged.

264

265 The high correlation values, the short positive time lags, and the increasing time lags with  
266 distance from the river observed from the cross-correlation analysis all suggest that  
267 piezometric levels in the floodplain are controlled by river stage fluctuations. However,  
268 this general pattern is variable in time and space. Figure 5 shows that there is a positive  
269 correlation between the time lag and the day of the year (DOY) on which the flood event  
270 occurred at four locations within the alluvial floodplain. The smallest time lags were  
271 recorded for the summer flood events (DOY 188 to 249). For all piezometers, a 50%  
272 increase in time lags between DOY 188 (7 July) and 336 (2 December) was observed.  
273 Although there is a general tendency to the increase of time lag throughout the summer,  
274 there is an opposite trend when several floods follow a period without precipitation event.  
275 Two “dry” periods occurred during this study, between DOY 205 and 230, and between  
276 DOY 250 and 320. For both periods, the first flood event has a significantly larger time  
277 lag and the time lag for each of the following storm events occurring after was relatively  
278 smaller. These “dry” periods resulted in a deeper unsaturated zone, which explain the  
279 significant increased time lags followed by decreased time lag.

280 The amplitude of groundwater fluctuations decreased with distance from the river  
281 (Figure 6). A damping effect can be seen, probably induced by the distance between  
282 the piezometer and the channel. All  $R^2$  values are higher than 0.92. This amplitude  
283 variability is not related to floodplain morphology. Comparing the three flood events  
284 revealed that amplitudes conserve similar proportions, e.g., water level amplitudes  
285 recorded at 21 m distance were always 60% higher than amplitudes recorded 250 m from  
286 the channel, regardless of flood magnitude. In addition, the amplitudes of groundwater  
287 fluctuations close to the channel can be higher than the amplitudes of river stage

288 fluctuations. For example, 21 m from the channel, the 0.37 m river level fluctuation  
289 recorded during the 26 August–3 September event and the 1.04 m river level fluctuation  
290 recorded during the 5–12 September event induced groundwater fluctuations of 0.40 m  
291 (108%) and 1.14 m (109%), respectively. Also, comparison of the 26 August – 3  
292 September event to 2–16 July event shows that a flood event of a lower magnitude (0.37  
293 m) and of a shorter rising limb (32.5 h) induces larger water level fluctuations than a  
294 flood event of a higher magnitude (0.42 m) with a longer rising limb (90.8 h). The  
295 amplitudes of groundwater fluctuations depend not only on the piezometer-channel  
296 distance and on the magnitude of the flood events, but also on the duration of the flood  
297 rising limb.

298

### 299 *3.2 Spatial analysis of groundwater level dynamics*

300 At the study site, the Matane River is generally a gaining stream, i.e., the hydraulic  
301 gradient indicates that flow is towards the river. To investigate if the spatial dynamics of  
302 hydraulic gradients is affected during a flood event, hourly groundwater equipotential  
303 maps were produced. These maps suggest that hydraulic gradients vary temporally and  
304 spatially during flood events and that they may reverse. Figure 7 shows that the water  
305 pressure exerted on the channel banks from stream flooding induced hydraulic gradient to  
306 change flow orientation during the 5–12 September flood. At  $22 \text{ m}^3 \text{ s}^{-1}$  on 5 September at  
307 00:00 am (Figure 7a), the Matane River was a gaining stream. The highest water level of  
308 59.20 m at piezometer D223 and the lowest water level of 58.37 m at piezometer D21  
309 indicate a west-oriented flow related to a hydraulic gradient of  $3.31 \text{ mm m}^{-1}$ . The  
310 hydraulic gradient indicated groundwater flow re-oriented towards the eastern valley

311 walls (Figure 7b) from 6 September 07:00 am ( $105 \text{ m}^3 \text{ s}^{-1}$ ) to 11:00 pm ( $187 \text{ m}^3 \text{ s}^{-1}$ ), even  
312 if the peak stream discharge of  $213 \text{ m}^3 \text{ s}^{-1}$  was at 02:00pm. Using hydraulic heads from  
313 piezometers D55 and D176, the steepest perpendicular hydraulic gradient obtained is  
314  $1.9 \text{ mm m}^{-1}$  and been recorded at 3:15 pm on 6 September. The hydraulic gradient  
315 returned to its initial orientation, i.e., gaining stream, at approximately 1:00pm on 7  
316 September (Figure 7c). At that time, the hydraulic gradient between D223 and D21 was  
317  $2.81 \text{ mm m}^{-1}$  and it is only on 8 September at 07:45 am that the hydraulic gradient at the  
318 field site returned to its pre-storm condition of  $3.31 \text{ mm m}^{-1}$ .

319

320 Based on the highest saturated soil hydraulic conductivity ( $8.48 \times 10^{-4} \text{ m s}^{-1}$ , piezometer  
321 D139 (table 1)), with the highest hydraulic gradient of  $1.98 \text{ mm m}^{-1}$  (observed at 3:15 pm  
322 on 6 September), and a typical value of 0.25 for the effective porosity (Freeze and  
323 Cherry, 1979), groundwater flow velocity through the floodplain during the inverted  
324 hydraulic gradient was  $2.41 \times 10^{-2} \text{ m h}^{-1}$ . However, cross-correlation analyses for the 5–12  
325 September flood event indicate an average propagation velocity of  $11.5 \text{ m h}^{-1}$ , i.e., two to  
326 three orders of magnitude higher than the estimated groundwater velocity. This suggests  
327 that hydraulic head fluctuations correspond to the propagation of a groundwater  
328 floodwave throughout the floodplain triggered by the river stage fluctuation. The 5–12  
329 September  $213 \text{ m}^3 \text{ s}^{-1}$  flood event is the only recorded event that induced a change in  
330 groundwater flow orientation of the alluvial aquifer during the study period. However, it  
331 is expected that larger flood events would induce similar processes.

332

333 In order to evaluate the floodwave propagation through the Matane river alluvial aquifer,  
334 hydraulic heads profiles from the stream through a transect of piezometers (D21, D81,  
335 and D176) during the 5-12 September flood were assessed throughout the duration of the  
336 flood (Figure 8). River levels used for the profiles come from the river stage gauge  
337 downstream (RSGdn) temporal series. Results indicate that as the stage in the river  
338 increased, the flow direction in the aquifer reversed. At the start of the flood pulse,  
339 Matane river is a gaining stream. At the peak of the flood pulse on 6 September 04:00pm,  
340 the groundwater flow orientation was towards the valley wall, indicating that the river  
341 water level was higher than that of the alluvial aquifer. As the flood pulse receded, the  
342 groundwater flow direction reverted back towards the stream. It should also be noted, that  
343 as the river stage started to fall from 6 September 08:00pm to 7 September 04:00am, the  
344 underground floodwave was still propagating through the floodplain, hydraulic gradient  
345 was still reversed and hydraulic heads kept rising at D81 and D176. This would, first,  
346 inform that a floodwave may propagates beyond the study site (> 250 m from the river),  
347 but also highlight that the floodplain has stored water almost to the exfiltration of the  
348 water table at the floodplain surface at D176 (59.51 m (Table 1)). It is finally on 7  
349 September at 08:00 am that both river stage and water levels were falling.

350

351

352 4. DISCUSSION

353 *4.1 Groundwater floodwave propagation*

354 This study highlights the effects of the Matane River discharge fluctuations on the water  
355 level of its alluvial aquifer. Field measurements suggest that a floodwave propagates  
356 through the gravelly floodplain over a spatial extent much larger than the hyporheic zone.  
357 Results also suggest that the alluvial aquifer of the Matane Valley is hydraulically  
358 connected and primarily controlled by river stage fluctuations, even at stream discharges  
359 below bankfull. It has been reported that river stage fluctuations in some catchments were  
360 the processes primarily responsible for groundwater fluctuations throughout a floodplain  
361 (Lewandowski et al., 2009; Vidon, 2012). Another study reports that piezometers distant  
362 from the channel reflect hillslope groundwater contributions (Jung et al., 2004). Here,  
363 cross-correlation results (Figure 3b) show lower correlations and much longer delays  
364 between precipitation and groundwater levels than between river levels and groundwater  
365 levels. It is clear that direct precipitation contributes to recharge the unconfined alluvial  
366 aquifer. However, this is not the primary process responsible for groundwater increases  
367 during the flood events, probably because of the unsaturated storage capacity.  
368 Lewandowski et al. (2009) showed that precipitation was responsible for 20% of the  
369 groundwater fluctuations in the River Spree floodplain whereas, Vidon (2012) noted also  
370 no significant correlation between precipitation and groundwater fluctuations,

371

372 The propagation of the hydraulic head fluctuations through alluvial aquifers during flood  
373 events has been discussed by several authors (Sophocleous, 1991; Jung et al., 2004;  
374 Lewandowski et al., 2009; Vidon, 2012). Jung et al. (2004) compared their results to a

375 kinematic wave propagation based on flux velocities. This was done on a nearly  
376 synchronous response of the groundwater to the river stage during in-bank conditions,  
377 and on a wave-like response of the groundwater induced by an increase in river stage.  
378 Kinematic wave theory (see Lighthill and Withman, 1955) is based on the law of mass  
379 conservation through the continuity equation and a flux-concentration and may be  
380 applicable over a wide range of hydrological processes (Singh, 2002). To be considered  
381 as kinematic, a wave must be nondispersive and nondiffusive, two conditions that are  
382 necessary for the conservation of its length and amplitude over time and throughout  
383 space. In contrast, Thual (2008) showed that a dispersive and diffusive wave is  
384 considered as a dynamic wave. The amplitude of a dynamic wave will decrease over time  
385 and throughout space, but its length will increase.

386

387 In this study, the propagation of an underground floodwave, triggered by the river stage  
388 fluctuations for all flood events, is interpreted as a dynamic wave propagating within the  
389 alluvial aquifer. This interpretation is based on the non-conservation of hydraulic head  
390 fluctuations over time and through space. The groundwater response to the pulse induced  
391 by the rising river stage is however delayed and damped through the floodplain, as noted  
392 in Vekerdy and Meijjerink (1998) and Lewandowski et al. (2009). Figure 9 is a  
393 representation of a dynamic wave propagation through the alluvial aquifer of the Matane  
394 floodplain for the 5–12 September flood event. Near the river, hydraulic head amplitudes  
395 are high but the duration of high hydraulic heads is short. As a groundwater floodwave  
396 propagates distant from the river, friction through the porous medium causes a loss of  
397 energy, which induces the damping effect. This damping effect causes water table

398 amplitudes to become smaller, but hydraulic heads to remain high longer, inducing the  
399 floodwave crest to migrate (Figure 9). Every flood event, independent of its magnitude,  
400 induced dynamic wave propagations, but it is only the September event that caused  
401 hydraulic gradient to change flow orientation.

402

403 The groundwater floodwave hypothesis is also supported by the fact that a streamflood  
404 event induces water levels to rise instead of creating a lateral groundwater mass  
405 displacement through the floodplain. The absence of a significant displacement of river  
406 water in the floodplain during a flood event is supported by the propagation velocities of  
407 the 5–12 September flood event that are 2-3 orders of magnitude higher (6.00 to 10.93  
408  $\text{m h}^{-1}$ ) than the groundwater velocity ( $10^{-2} \text{ m h}^{-1}$ ) measured at the highest reversed  
409 hydraulic gradient of the field site ( $1.9 \text{ mm m}^{-1}$ ) on 6 September at 3:15 pm. These results  
410 support those of Vidon (2012), who reported propagation velocities three orders of  
411 magnitude higher than groundwater velocities, which were in the range of  $10^{-4} \text{ m h}^{-1}$ .  
412 Jung et al. (2004) reported propagation velocities five to six orders higher than flux  
413 velocities of  $10^{-4}$ - $10^{-5} \text{ m h}^{-1}$ , whereas Lewandowski et al. (2009) noted the propagation of  
414 pressure fluctuations approximately 1000 times faster than groundwater flow. Figure 5  
415 shows an increase in the time lag throughout the year induced by a long period of  
416 groundwater discharging to the river between the 5–12 September and the 10–26  
417 November flood events. This increase in the time lag represents not only a reduction of  
418 propagation velocities through the year, but also highlights the effects of prior  
419 unsaturated zone. Propagation velocities are not correlated with rainfall intensity. If  
420 rainfall intensity affected time lags, a large variability of time lags between piezometers

421 would not be observed at each flood event, nor would it be observed for similar rainfall  
422 intensities.

423

424 Streamfloods can affect the local groundwater flow directions in the floodplain  
425 depending on the flood magnitude. Potentiometric maps (Figure 7) show that the  
426 hydraulic gradient within the floodplain reversed at a stream discharge of  $95 \text{ m}^3 \text{ s}^{-1}$  during  
427 the 5–12 September flood event. Some researchers have reported reversed hydraulic  
428 gradients and the development of a groundwater ridge toward valley walls capable of  
429 ‘switching off’ hillslope inputs during a streamflood with a stream discharge below  
430 bankfull, sometimes for long periods (e.g. Burt et al., 2002; Vidon, 2012). Here, the 5–12  
431 September event is the only event that induced a groundwater flow reversal which lasted  
432 16 h before returning to pre-storm initial hydraulic gradient three days later.

433

#### 434 *4.2 Groundwater flooding*

435 The occurrence of groundwater flooding in floodplain environments is controlled by the  
436 degree of connectivity between a stream and its alluvial aquifer (Mardhel et al., 2007;  
437 Cobby et al., 2009). Figure 8 shows that groundwater levels rise almost synchronously as  
438 the river stage rises. But to determine the range of stream discharges at which exfiltration  
439 is likely to occur at study site, linear regression analyses for each piezometer were  
440 calculated using highest hydraulic heads reached below floodplain surface and the peak  
441 flow of recorded flood events (Figure 10a). Strong correlations ( $R^2 > 0.96$ ) exist for all  
442 piezometers, taking account the  $213 \text{ m}^3 \text{ s}^{-1}$  event or not. For example, the  $213 \text{ m}^3 \text{ s}^{-1}$   
443 during the 5–12 September event induced the hydraulic head to rise to 9 cm below the

444 surface at D176 and to 15 cm below the surface at D21 and D81. The hydraulic heads  
445 rose closest to the floodplain surface at piezometers installed in the oxbow feature.  
446 Figure 10b shows the spatial distribution of the predicted stream discharges producing  
447 exfiltration at the study site. By extrapolating from the water level depths-flowrates  
448 relations, it is possible to estimate that exfiltration would occur at stream discharges  
449 ranging between 238 and 492 m<sup>3</sup> s<sup>-1</sup> depending on the location within the floodplain.  
450 Figure 10b shows that the lowest predicted stream discharges would induce flooding at  
451 the lowest part of the floodplain (i.e., in the oxbow), and at piezometers D55 and D175  
452 only stream discharges higher than bankfull would induce exfiltration of the water table.  
453 Estimated bankfull discharge of the Matane River is 350 m<sup>3</sup> s<sup>-1</sup>, so according to the  
454 models, exfiltration occurs at stream discharges well below bankfull. The range of stream  
455 discharges that took place during the study period were all below the extrapolated  
456 exfiltration thresholds supporting the fact that no exfiltration event was observed.  
457 Although the exfiltration thresholds would need validation, the data strongly indicate that  
458 river stage levels and underground floodwave propagation can contribute to groundwater  
459 flooding. Further developments in the estimation of groundwater flooding river flow rates  
460 should consider the initial hydraulic heads before stream floods occurred, the spatial  
461 connectivity between piezometers by runoff at the floodplain's surface once exfiltration  
462 occurred, or a possible overflow of the Matane River.

463

464 5. CONCLUSION

465 This study shows that water level fluctuations in the Matane alluvial floodplain are  
466 primarily governed by river stage fluctuations. The amplitudes of groundwater  
467 fluctuations depend on the distance from the channel, on the flood magnitude, and on the  
468 rising limb of the flood. The largest flood event recorded during the study period is the  
469 only event that influenced local groundwater flow orientation within the alluvial  
470 floodplain by generating an inversion of the hydraulic gradient toward the valley walls  
471 for sixteen hours. The results also show a damping effect of the groundwater response  
472 related to the distance of piezometers from the channel. Every flood event showed a large  
473 variability of lag values across the floodplain. The periods of groundwater discharging to  
474 the river of July and October 2011 caused time lags to increase for next flood events.  
475 Exfiltration of groundwater is predicted for stream discharges that can be well below  
476 bankfull. However, these estimations do not take into account the spatial connectivity  
477 between piezometers, the initial depth of the groundwater, or a possible overflow of the  
478 river. Finally, this study reveals that the pressure exerted on the river bank by a stream  
479 flood induces the propagation of a groundwater floodwave, interpreted as a dynamic  
480 wave, for all the studied floods. The propagation speed remains relatively constant across  
481 the floodplain but depends on the initial conditions within the floodplain. Propagation of  
482 groundwater level fluctuations occurs at every event, but only the largest event in this  
483 study affected groundwater flow directions. This study supports the idea that a river flood  
484 has a much larger effect in time and space than what is occurring within the channel.  
485 Further research including groundwater geochemistry would bring insights on energy  
486 exchange processes through the river bank and allow to determine whether and to what  
487 distance surface water reaches the floodplain below ground the during flood events.

488

489 ACKNOWLEDGEMENTS

490 This research was financially supported by the climate change consortium Ouranos as  
491 part of the “Fonds vert” for the implementation of the Quebec Government Action Plan  
492 2006-2012 on climate change, by BORÉAS, by the Natural Sciences and Engineering  
493 Research Council of Canada (NSERC), by the Centre d’Études Nordiques, and by the  
494 Fondation de l’UQAR. We are thankful to several team members of the Laboratoire de  
495 recherche en géomorphologie et dynamique fluviale de l’UQAR for field assistance.

496

497 REFERENCES

- 498 Barlow, J.R., Coupe, R.H., 2009. Use of heat to estimate streambed fluxes during  
499 extreme hydrologic events. *Water Resour. Res.* 45 (1), 1-10, doi: 566  
500 10.1029/2007WR006121.
- 501 Burt, T.P., Bates, P.D., Stewart, M.D., Claxton, A.J., Anderson, M.G., Price, D.A., 2002.  
502 Water table fluctuations within the floodplain of the River Severn, England. *J. Hydrol.*  
503 262 (1–4), 1–20.
- 504 Cardenas, M.B., 2008. The effect of river bend morphology on flow and timescales of  
505 surface water-groundwater exchange across pointbars. *J. Hydrol.* 362 (1–2), 134–141.
- 506 Cobby, D., Morris, S., Parkes, A., Robinson, V., 2009. Groundwater flood risk  
507 management: advances towards meeting the requirements of the EU floods directive. *J.*  
508 *Flood Risk Manag.* 2 (2), 111–119.
- 509 Freeze, R.A., Cherry, J.A., 1979. *Groundwater*. Prentice Hall, Englewood Cliff.
- 510 Gillham, R.W., 1984. The capillary fringe and its effect on water-table response. *J.*  
511 *Hydrol.* 67, 307–324.
- 512 Gooseff, M.N., 2010. Defining hyporheic zones – Advancing our conceptual and  
513 operational definitions of where stream water and groundwater meet. *Geo. Compass* 4  
514 (8), 945–955.
- 515 Haycock, N.E, Burt, T.P., 1993. Role of floodplain sediments in reducing the nitrate  
516 concentration of subsurface run-off : a case study in the Cotswolds, UK. *Hydrol.*  
517 *Processes* 7, 287-295.

518 Hammer, Ø., Harper, D.A.T., Ryan, P.D., 2001. PAST: Paleontological statistics  
519 software package for education and data analysis. *Palaeontologia Electronica* , 4 (1), 9.

520 Harvey, J.W., Bencala, K.E., 1993. The effect of streambed topography on surface–  
521 subsurface water exchange in mountain catchments. *Water Resour. Res.* 29 (1), 89–98,  
522 doi: 10.1029/92WR01960.

523 Harvey, J. W., J. D. Drummond, R. L. Martin, L. E. McPhillips, A. I. Packman, D. J.  
524 Jerolmack, S. H. Stonedahl, A. Aubeneau, A. H. Sawyer, L. G. Larsen, and C. Tobias,  
525 2012, Hydrogeomorphology of the hyporheic zone: Stream solute and fine particle  
526 interactions with a dynamic streambed. *J. Geo. Res. - Biogeosciences*, Volume 117,  
527 G00N11, doi:10.1029/2012JG002043.

528 Hvorslev, M.J., 1951. Time lag and soil permeability in groundwater observation. U.S.  
529 Army Corps of Engineers, Waterways Experimental Station, Vicksburg, Miss., Bulletin  
530 365.

531 Jung, M.T., Burt, T.P., Bates, P.D., 2004. Toward a conceptual model of floodplain water  
532 table response. *Water Resour. Res.* 40 (12), 1–13.

533 Kreibich, H., Thielen, A., 2008. Assessment of damage caused by high groundwater  
534 inundation. *Water Resour. Res.* 44 (9), W09409, doi:10.1029/2007WR006621.

535 Lebuis, J., 1973. *Geologie du Quaternaire de la region de Matane-Amqui- Comtes de*  
536 *Matane et de Matapedia. Rapport DPV-216, Ministere des Richesses naturelles, Direction*  
537 *generale des Mines, Gouvernement du Quebec, Quebec, 18.*

538 Lewandowski, J., Lischeid, G., Nützmann, G., 2009. Drivers of water level fluctuation  
539 and hydrological exchange between groundwater and surface water at the lowland river  
540 Spree (Germany): field study and statistical analyses. *Hydrol. Processes* 23 (15), 2117–  
541 2128.

542 Lighthill M.J., Whitham, G.B., 1955. On kinematic waves: 1. Flood movement in long  
543 rivers. *Proceedings of the Royal Society London, Series A* 229, 281–316.

544 Mardhel, V., Pinault, J.L., Stollsteiner, P., Allier, D., 2007. Etude des risques  
545 d'inondation par remontees de nappe sur le bassin de la Maine, Rapport 55562-FR,  
546 Bureau de recherches geologiques et minieres, 156.

547 Mertes, L.A., 1997. Documentation and significance of the perirheic zone on inundated  
548 floodplains. *Water Resour. Res.* 33 (7), 1749–1762.

549 Pinault, J.L., Amraoui, N., Golaz, C., 2005. Groundwater-induced flooding in macropore-  
550 dominated hydrological system in the context of climate changes. *Water Resour. Res.* 41  
551 (5), 1–16.

552 Singh, V.P., 2002. Is hydrology kinematic? *Hydrol. Processes*, 16 (3), 667–716.

553 Sophocleous, M.A., 1991. Stream-floodwave propagation through the great bend alluvial  
554 aquifer, Kansas: Field measurements and numerical simulations. *J. Hydrol.* 124 (3–4),  
555 207–228.

556 Stonedahl, S.H., Harvey, J.W., Wörman, A., Salehin, M., Packman, A.I., 2010. A  
557 multiscale model for integrating hyporheic exchange from ripples to meanders. *Water*  
558 *Resour. Res.* 46, 1–14, doi:10.1029/2009WR008865.

559 Thual, O., 2008. Propagation de l'onde de crue, in Thual, O. (Ed.), Hydrodynamique de  
560 l'Environnement. Les Editions de l'Ecole Polytechnique, Toulouse, pp.131-157.

561 Triska, F.J., Kennedy, V.C., Avanzio, R.J., Zellweger, G.W., Bencala, K.E., 1989.  
562 Retention and transport of nutrients in a third-order stream in northwestern California:  
563 Hyporheic processes. *Ecology*, 70 (6), 1893–1905.

564 Vekerdy, Z., Meijerink, A.M.J., 1998. Statistical and analytical study of the propagation  
565 of flood-induced groundwater rise in an alluvial aquifer. *J. Hydrol.*, 205 (1–2), 112–125.

566 Vidon, P., 2012. Towards a better understanding of riparian zone water table response to  
567 precipitation: surface water infiltration, hillslope contribution or pressure wave  
568 processes? *Hydrol. Processes*, 26 (21), 3207–3215.

569 Woessner, W., 2000. Stream and fluvial plain interactions: rescaling hydrogeologic  
570 thought. *Groundwater*, 38 (3), 423–429.

571 Wondzell, S.W., Gooseff, M.M., 2013, Geomorphic controls on hyporheic exchange  
572 across scales: watersheds to particles, in Shroder, J. F. (Ed.), *Treatise in Geomorphology*.  
573 Academic Press, San Diego, pp. 203-218.

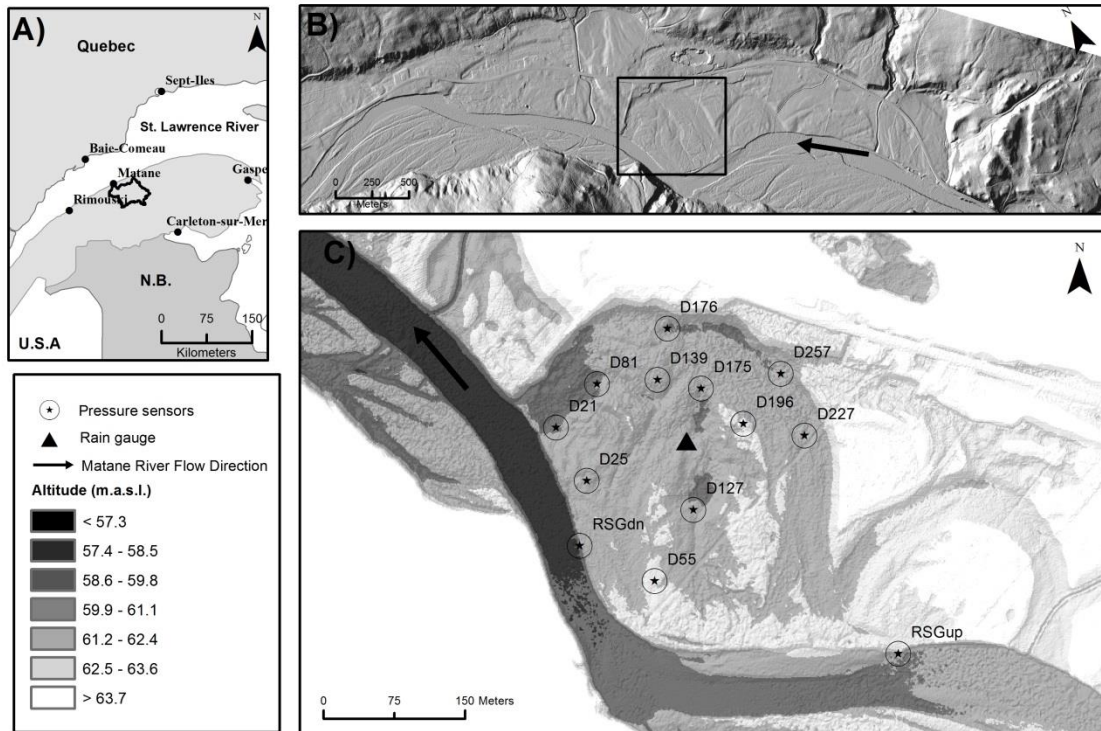
574

575 **Table 1:** Hydraulic conductivity values derived from slug tests.

Piezometer	Floodplain elevation (m)	$K$ ( $\text{m s}^{-1}$ )
D21	59.65	$1.99 \times 10^{-4}$
D25	60.55	$1.94 \times 10^{-4}$
D55	61.17	$2.78 \times 10^{-4}$
D81	59.61	$6.61 \times 10^{-4}$
D139	60.82	$8.48 \times 10^{-4}$
D175	60.03	$6.18 \times 10^{-4}$
D176	59.51	$2.10 \times 10^{-5}$
D196	61.03	$1.95 \times 10^{-4}$
D223	60.31	$2.07 \times 10^{-4}$
D257	60.02	$8.90 \times 10^{-5}$

576

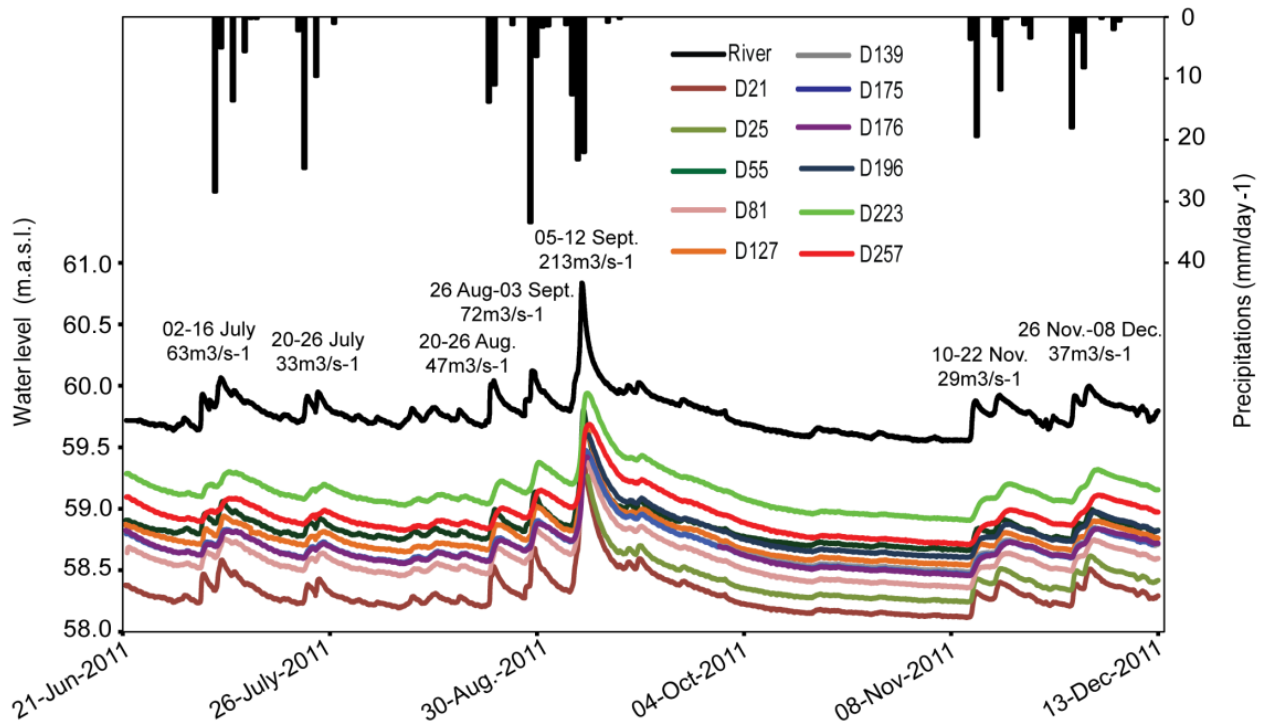
577



579

580 Figure 1 : (A) Location of the the Matane River Basin, Quebec, Canada; (B) Location of  
 581 the study site within a coarse sand gravelly floodplain constructed by fluvial dynamics;  
 582 (C) Position of the piezometers within the study site. Piezometers with pressure sensors  
 583 are indicated. The names of the piezometers reflect the perpendicular distance to the  
 584 Matane River.

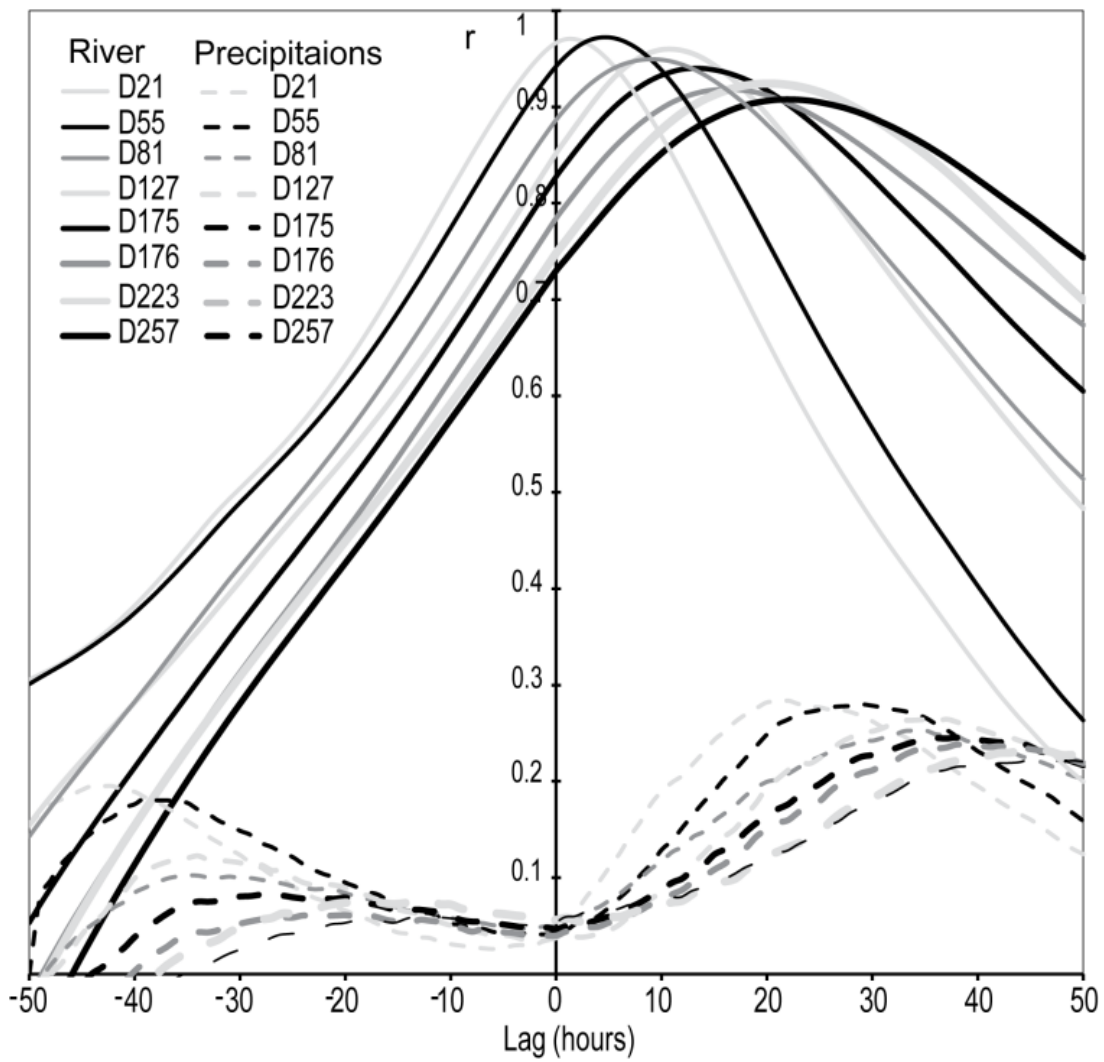
585



586

587 Figure 2 : Water levels and river stage time series from 21 June to 12 December 2011.

588



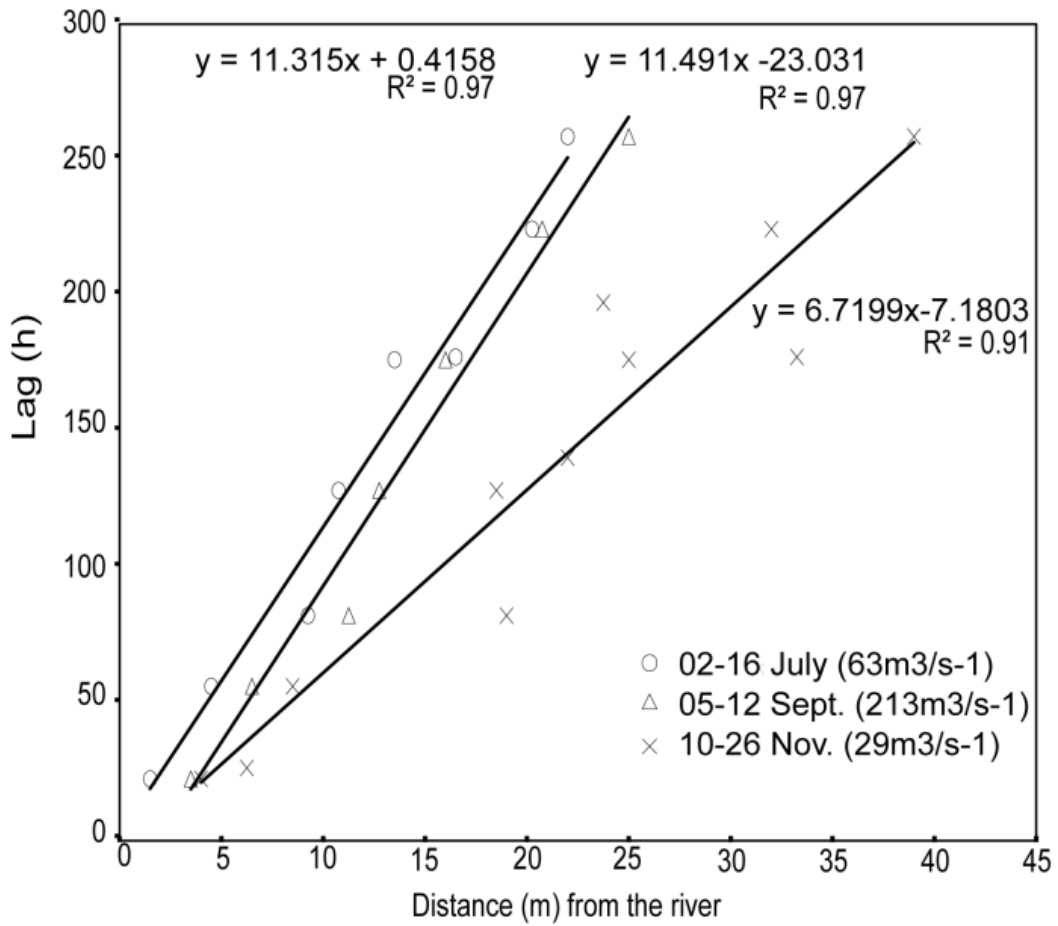
589

590 Figure 3 : Cross-correlation functions using river levels as input and groundwater levels

591 as output (solid lines) and precipitation as input and groundwater levels as output (dashed

592 lines).

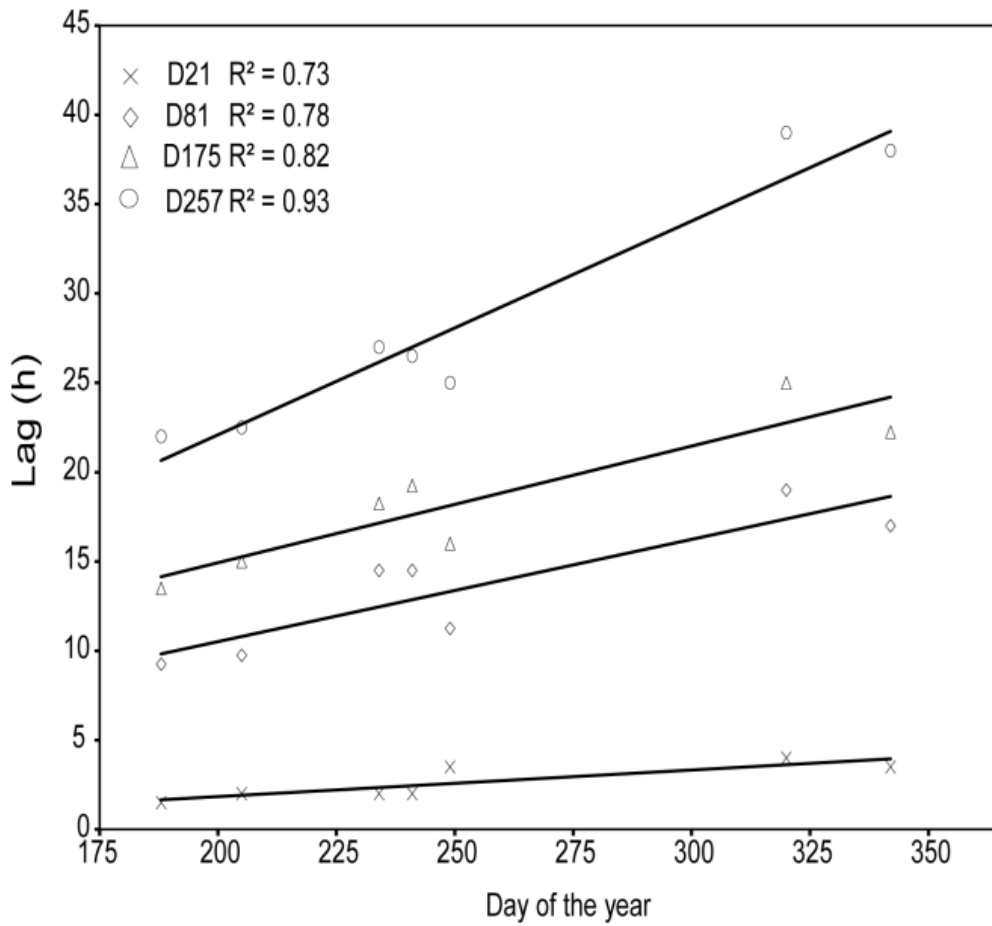
593



594

595 Figure 4 : Time lags of piezometers as a function of distance from the river for three  
 596 selected flood events.

597

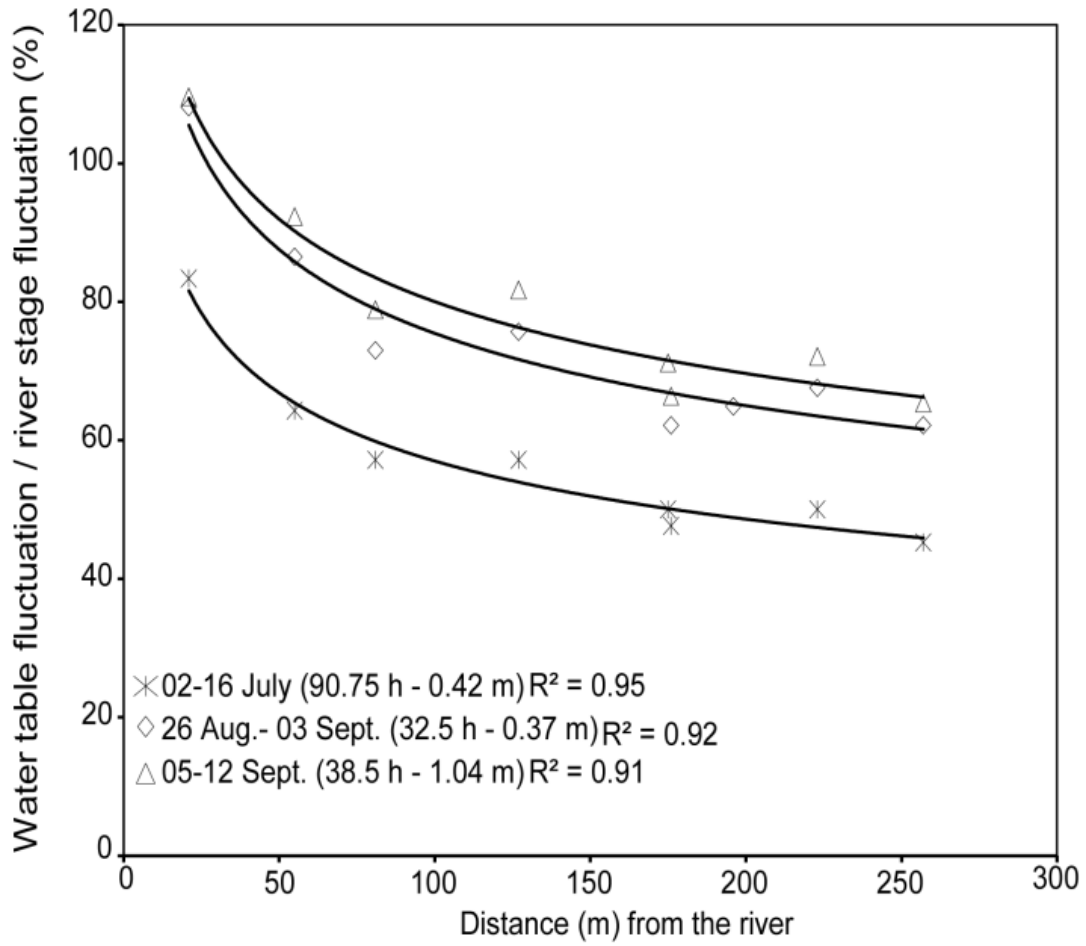


598

599 Figure 5 : Time lags as a function of day of the year of flood occurrence at four selected  
 600 positions within the alluvial floodplain.

601

602

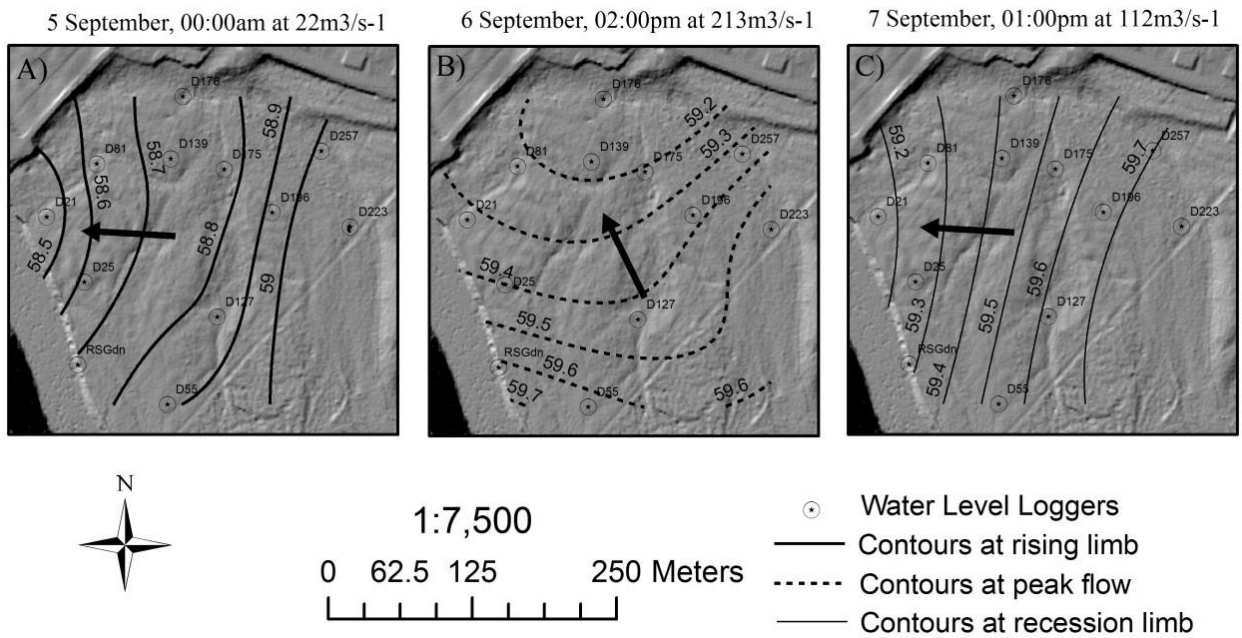


603

604 Figure 6 : Water level fluctuations within the floodplain for three flood events. Values

605 parenthesis indicate duration of flood pulse rising limb and flood even magnitude.

606



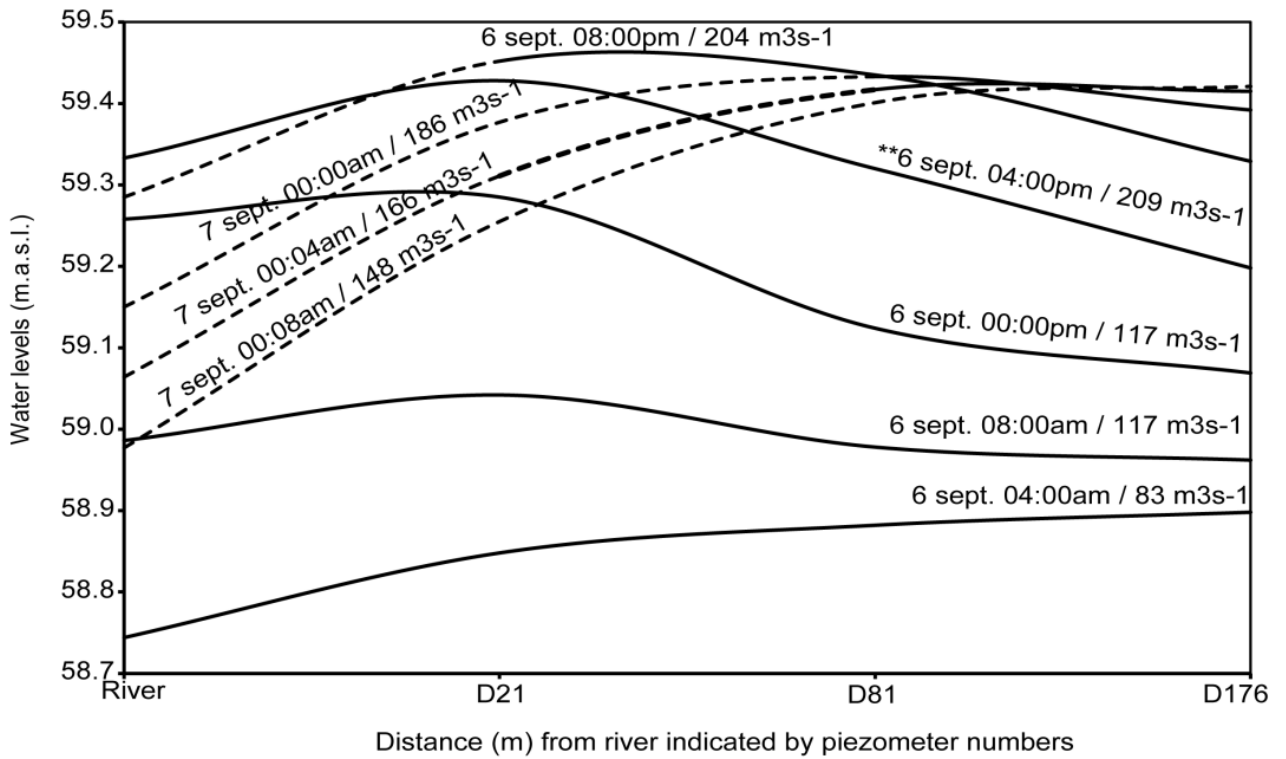
607

608 Figure 7 : Groundwater flow directions suggested from the equipotential lines during 5–

609 12 September event.

610

611



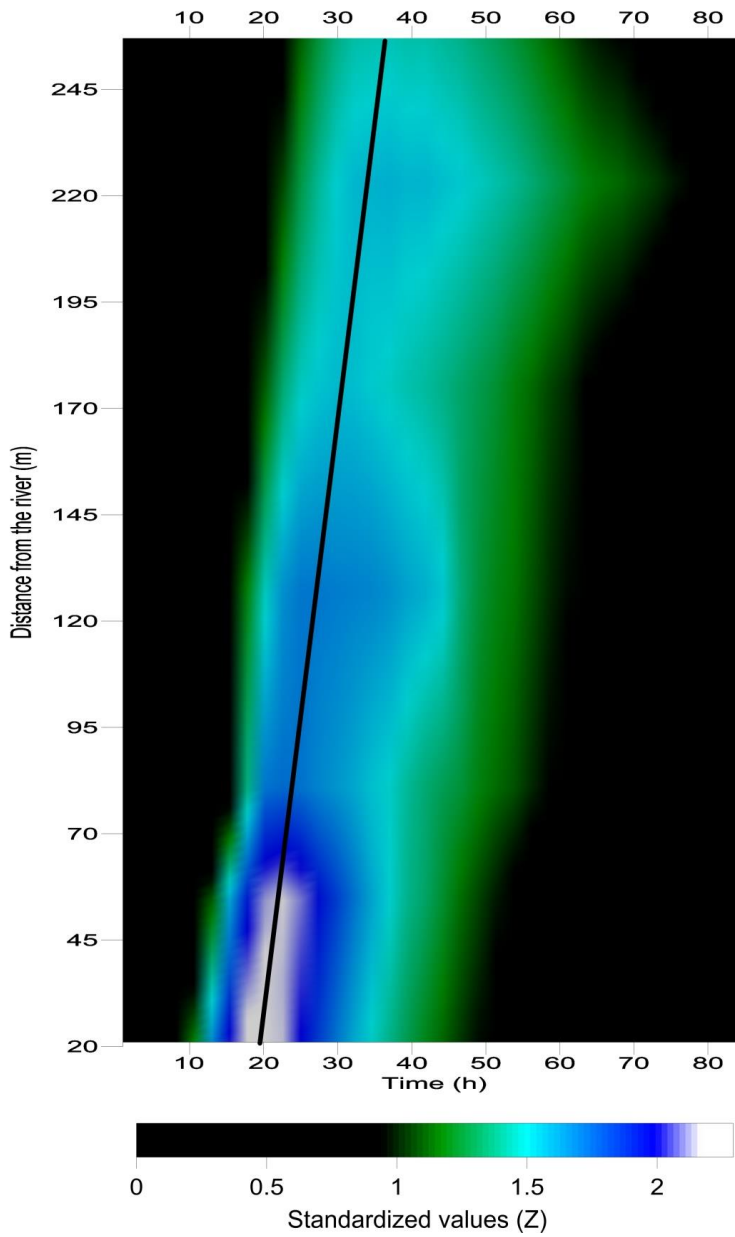
612

613 Figure 8 : Propagation of a groundwater floodwave within the aquifer during the 5–12

614 September flood event. Solid lines indicate rising river stage and water levels and dashed lines

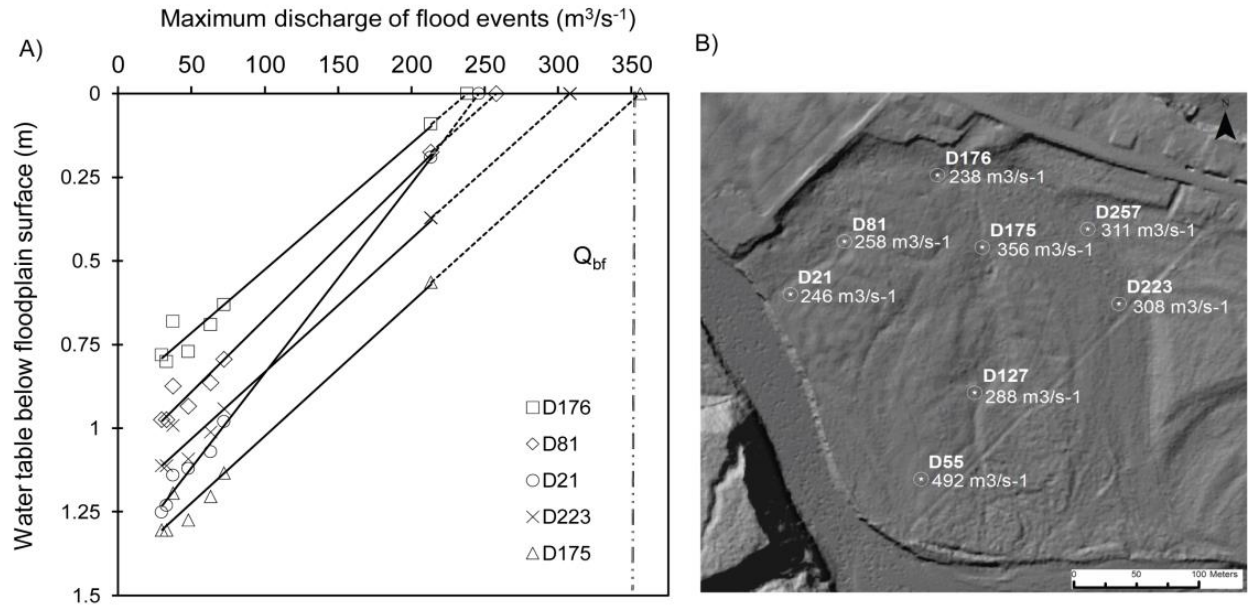
615 indicate falling river stage and water levels . \*\* maximum river stage.

616



617

618 Figure 9 : Floodwave propagation within the floodplain for the 5–12 September  $213 \text{ m}^3\text{s}^{-1}$   
 619 flood event using the standardized water level from piezometers D21, D55, D81, D127,  
 620 D175, D223 and D257. Step time is hourly from 6 September, 00:00 am. The black line  
 621 represents the groundwater floodwave crest displacement.



622

623 Figure 10 : Predicted stream discharges for exfiltration. (a) Regression model of  
 624 predicted exfiltration discharge for selected piezometers; (b) spatial distribution of the  
 625 predicted exfiltration discharges. Regression dashed lines correspond to extrapolation.  
 626 Vertical dashed line correspond to Matane river bankfull discharge.